J|A|C|S
ARTICLES
Published on Web 01/05/2006

Helical Conformational Dynamics and Photoisomerism of Alternating Pyridinedicarboxamide/*m*-(Phenylazo)azobenzene Oligomers

Chenyang Tie, Judith C. Gallucci, and Jon R. Parquette*

Contribution from the Department of Chemistry, The Ohio State University, Columbus, Ohio 43210

Received July 14, 2005; Revised Manuscript Received November 18, 2005; E-mail: parquett@chemistry.ohio-state.edu

Abstract: Alternating sequences of pyridine-2,6-dicarboxamides and *meta*-(phenylazo)azobenzenes have been assembled into oligomers composed of four (**8**) and eight (**9**) azobenzene linkages. X-ray crystallography confirmed that oligomer **8** adopts a two-turn helical conformation with a helical pitch of approximately 3.4 Å in the solid state. The presence of a two- and four-turn helical conformation of **8** and **9**, respectively, in polar and nonpolar solvents was elucidated by the anisotropic upfield shifting of protons located within the helices, NOE enhancements between protons oriented toward the helix interior, and the diastereotopicity of the terminal benzyloxycarbonyl (CBz) methylene protons. ^{1}H NMR line shape analysis of the CBz methylene hydrogens at the chain ends revealed a dynamic equilibria interconverting *M* and *P* helical conformations with energetic barriers ($\Delta G^{\ddagger}$) of 11.1 ($\Delta S^{\ddagger} = -19.4 \pm 1.6$ cal mol^{-1} K^{-1}; $\Delta H^{\ddagger} = 6.5 \pm 0.4$ kcal/mol) for **8** and 13.8 kcal/mol ($\Delta S^{\ddagger} = -6.6 \pm 6.2$ cal mol^{-1} K^{-1}; $\Delta H^{\ddagger} = 11.8 \pm 1.8$ kcal/mol) for **9**. Irradiation of the oligomers with 350 nm light induces an $E \rightarrow Z$ isomerization of the azo linkages that decreases in efficacy at longer helix lengths. The suppression of $E \rightarrow Z$ isomerization is a consequence of the contrasting behavior of the azo linkages located at the helix termini, which afford *Z*/*E* ratios similar to those of model compound **7d**, and the internal azo groups, which undergo significantly lower *Z*/*E* conversion ratios compared with **7e**.

Introduction

The interdependence of structure and function in biological systems[1] provides tremendous impetus for the design of unnatural oligomers that adopt compact, folded conformations resembling natural secondary structure.[2] In these natural systems, highly dynamic conformational processes serve to correlate local and global structural motions.[3] Understanding the nature of this conformational interplay in synthetic systems will be important for progress toward functional systems to be fully realized.[4] Therefore, the development of folded abiotic systems that respond to external stimuli represents a particularly important objective in the search for function.[5] Accordingly, intrinsically helical polymers and oligomers have been shown to experience *M*−*P* helical and helical−nonhelical conformational transitions following a structural perturbation.[6] However, the polydisperse nature of polymeric systems complicates analysis of the structural source of the conformational changes. The design of discrete folded oligomers composed of isomerizable repeat units should facilitate studies directed at understanding the delicate interplay between local and global conformational dynamics and structure. Recent studies in folded oligomers have shown that conformational perturbations induced by protonation,[7] metal coordination,[8] changes in solvent polarity,[9,10] and anion[11] or cation[12] binding effect corresponding changes in structure.

(1) Creighton, T. E. *Proteins: Structures and Molecular Properties*, 2nd ed.; W. H. Freeman: New York, 1993.
(2) For some reviews, see: (a) Licini, G.; Prins, L. J.; Scrimin, P. *Eur. J. Org. Chem.* **2005**, 969−977. (b) Huc, I. *J. Org. Chem.* **2004**, *69*, 17−29. (c) Sanford, A. R.; Yamato, K.; Yang, X.; Yuan, L.; Han, Y.; Gong, B. *Eur. J. Biochem.* **2004**, *271*, 1416−1425. (d) Cheng, R. P. *Curr. Opin. Struct. Biol.* **2004**, *14*, 512−520. (e) Martinek, T. A.; Fueloep, F. *Eur. J. Biochem.* **2003**, *270*, 3657−3666. (f) Sanford, A. R.; Gong, B. *Curr. Org. Chem.* **2003**, *7*, 1649−1659. (g) Hill, D. J.; Mio, M. J.; Prince, R. B.; Hughes, T. S.; Moore, J. S. *Chem. Rev.* **2001**, *101*, 3893−4012. (h) Cubberley, M. S.; Iverson, B. L. *Curr. Opin. Chem. Biol.* **2001**, *5*, 650−653. (i) Gellman, S. H. *Acc. Chem. Res.* **1998**, *31*, 173−180.
(3) (a) Mayer, K. L.; Earley, M. R.; Gupta, S.; Pichumani, K.; Regan, L.; Stone, M. J. *Nat. Struct. Biol.* **2003**, *10*, 962−965. (b) Kern, D.; Zuiderweg, E. R. P. *Curr. Opin. Struct. Biol.* **2003**, *13*, 748−757.
(4) Lockman, J. W.; Paul, N. M.; Parquette, J. R. *Prog. Polym. Sci.* **2005**, *30*, 423−452.
(5) (a) Balzani, V.; Credi, A.; Raymo, F. M.; Stoddart, J. F. *Angew. Chem., Int. Ed.* **2000**, *39*, 3348−3391. (b) Shinkai, S.; Ikeda, M.; Sugasaki, A.; Takeuchi, M. *Acc. Chem. Res.* **2001**, *34*, 494−503. (c) Takeuchi, M.; Ikeda, M.; Sugasaki, A.; Shinkai, S. *Acc. Chem. Res.* **2001**, *34*, 865−873. (d) Kovbasyuk, L.; Kraemer, R. *Chem. Rev.* **2004**, *104*, 3161−3188.
(6) (a) Borovkov, V.; Hembury, G. A.; Inoue, Y. *Angew. Chem., Int. Ed.* **2003**, *42*, 5310−5314. (b) Morino, K.; Maeda, K.; Yashima, E. *Macromolecules* **2003**, *36*, 1480−1486. (c) Hill, D. J.; Moore, J. S. *Proc. Natl. Acad. Sci. U.S.A.* **2002**, *99*, 5053−5057. (d) Egan, V.; Bernstein, R.; Hohmann, L.; Tran, T.; Kaner, R. B. *Chem. Commun.* **2001**, 801−802. (e) Nakashima, M.; Fujiki, J. R.; Koe, M.; Motonaga, S. E. *J. Am. Chem. Soc.* **2001**, *123*, 1963−1969. (f) Nakako, H.; Nomura, R.; Masuda, T. *Macromolecules* **2001**, *34*, 1496−1502. (g) Fujiki, M. *J. Am. Chem. Soc.* **2000**, *122*, 3336−3343. (h) Boiadjiev, S. E.; Lightner, D. A. *J. Am. Chem. Soc.* **2000**, *122*, 378−383.
(7) (a) Kanamori, D.; Okamura, T.-a.; Yamamoto, H.; Ueyama, N. *Angew. Chem., Int. Ed.* **2005**, *44*, 969−972. (b) Dolain, C.; Maurizot, V.; Huc, I. *Angew. Chem., Int. Ed.* **2003**, *42*, 2738−2740. (c) Kolomiets, E.; Berl, V.; Odriozola, I.; Stadler, A.-M.; Kyritsakas, N.; Lehn, J.-M. *Chem. Commun.* **2003**, 2868−2869.
(8) (a) Stone, M. T.; Moore, J. S. *J. Am. Chem. Soc.* **2005**, *127*, 5928−5935. (b) Stadler, A.-M.; Kyritsakas, N.; Lehn, J.-M. *Chem. Commun.* **2004**, 2024−2025. (c) Barboiu, M.; Lehn, J.-M. *Proc. Natl. Acad. Sci. U.S.A.* **2002**, *99*, 5201−5206. (d) Prince, R. B.; Okada, T.; Moore, J. S. *Angew. Chem., Int. Ed.* **1999**, *38*, 233−236.

 10.1021/ja0547228 CCC: $33.50

Scheme 1 [a]

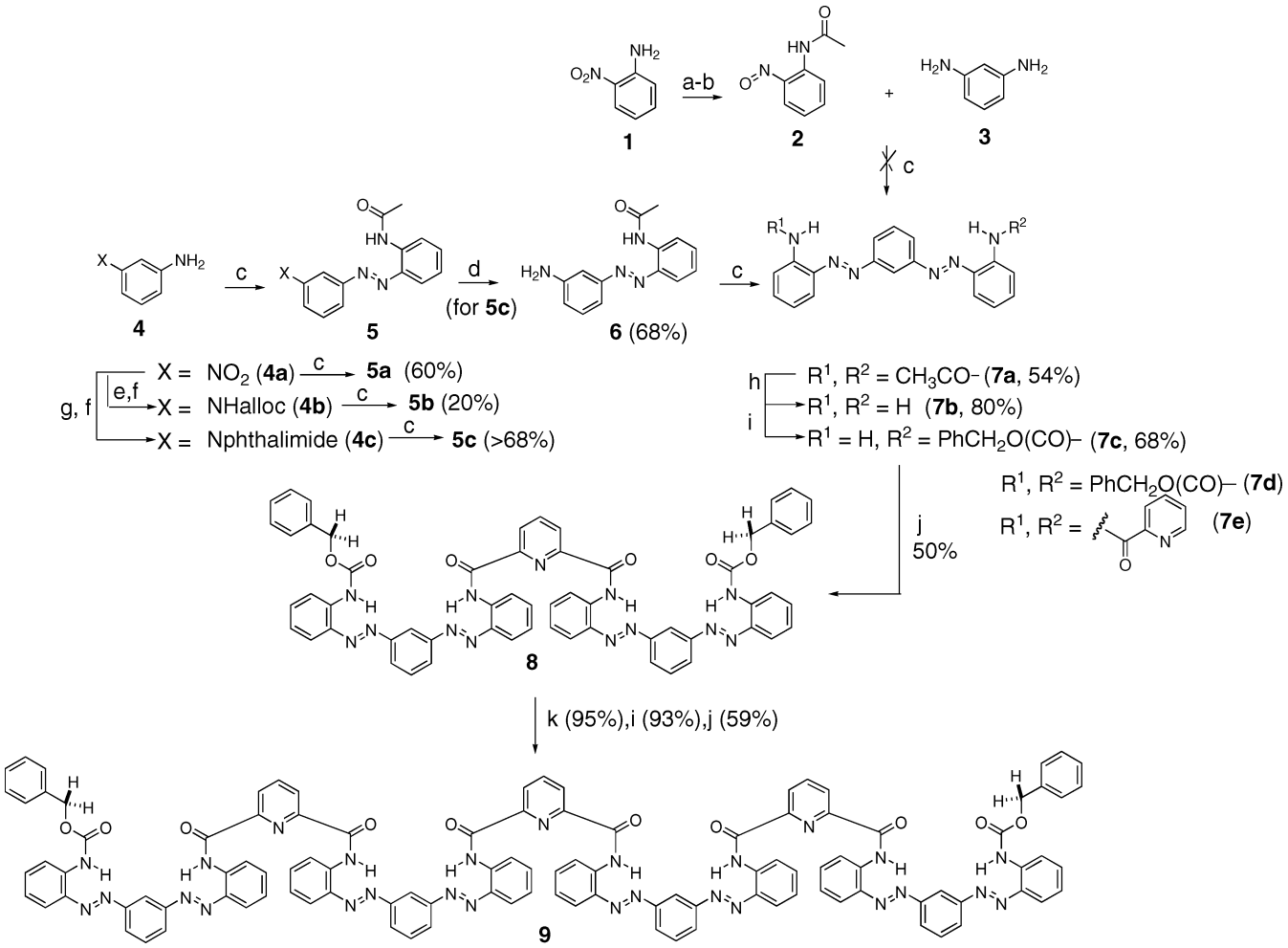

[a] Conditions: (a) Ac_2O, pyridine, HOAc, 99%; (b) NH_2NH_2, Rh/C, THF, then *t*-C_4H_9OCl, 88%; (c) **2**, HOAc, 100 °C; (d) 40% aq. $MeNH_2$, THF−MeOH (68% from **4c**); (e) allylchloroformate, Et_3N, toluene; (f) $SnCl_2$, EtOAc−MeOH; (g) phthalic anhydride, Et_3N, toluene, 82%; (h) KOH, EtOH−H_2O; (i) benzyl chloroformate, NaOH, CH_2Cl_2; (j) 4 Å sieves, pyridine, CH_2Cl_2, pyridine-2,6-dicarbonyl dichloride; (k) thioanisole, trifluoroacetic acid.

However, the photoisomerism of discrete azobenzene oligomers that adopt helical conformations in solution remains as an unexplored strategy to study the local−global interplay in folded systems. The goal of this work is to understand how azobenzene isomerism can modulate the properties of folded oligomers and, conversely, how structure impacts this isomerism when the azo function is embedded within the folded backbone of the system. Herein, we report the design, synthesis, and conformational properties of a discrete azobenzene oligomer constructed with up to eight azobenzene linkages that folds into a highly stable helical conformation in the *E* form.

The photochemical $E \rightarrow Z$ isomerization of azobenzene derivatives[13] has been exploited extensively to modulate the conformational and biological properties of folded peptides[14] and helical polymers.[15] In these systems, the $E \rightarrow Z$ transition either disrupts, changes, or enhances the secondary structure present within such polymers. Similarly, the photoisomerization of azobenzenes has been exploited to modulate the functional properties of crown ethers[16] and cyclodextrins,[17] supramolecular assemblies,[18] and the hydrodynamic volumes of dendrimers.[19] Although these effects have been imparted by incorporating the azobenzene function as a side chain or as an unfolded backbone connector of the peptide or polymer, there is no information concerning the effect of utilizing an azobenzene chromophore

(9) Nelson, J. C.; Saven, J. G.; Moore, J. S.; Wolynes, P. G. *Science* **1997**, *277*, 1793−1796.
(10) Hofacker, A. L.; Parquette, J. R. *Angew. Chem., Int. Ed.* **2005**, *44*, 1053−1057.
(11) (a) Goto K.; Moore, J. S. *Org. Lett.* **2005**, *7*, 1683−1686. (b) Chang, K.-J.; Kang, B.-N.; Lee, M.-H.; Jeong, K.-S. *J. Am. Chem. Soc.* **2005**, *127*, 12214−12215. (c) Sanchez-Quesada, J.; Seel, C.; Prados, P.; de Mendoza, J. *J. Am. Chem. Soc.* **1996**, *118*, 277−278.
(12) (a) Petitjean, A.; Nierengarten, H.; van Dorsselaer, A.; Lehn, J.-M. *Angew. Chem., Int. Ed.* **2004**, *43*, 3695−3699. (b) Petitjean, A.; Cuccia, L. A.; Lehn, J.-M.; Nierengarten, H.; Schmutz, M. *Angew. Chem., Int. Ed.* **2002**, *41*, 1195−1198.
(13) Rau, H. Azo Compounds. In *Studies in Organic Chemistry: Photochromism. Molecules and Systems*; Durr, H., Bonas-Laurent, H., Eds.; Elsevier: Amsterdam, 1990; Vol. 40, pp 165−192.
(14) (a) Renner, C.; Kusebauch, U.; Loeweneck, M.; Milbradt, A. G.; Moroder, L. *J. Pept. Res.* **2005**, *65*, 4−14. (b) Pieroni, O.; Fissi, A.; Angelini, N.; Lenci, F. *Acc. Chem. Res.* **2001**, *34*, 9−17. (c) Willner, I.; Rubin, S. *Angew. Chem., Int. Ed. Engl.* **1996**, *35*, 367−385.
(15) (a) Natansohn, A.; Rochon, P. *Chem. Rev.* **2002**, *102*, 4139−4175. (b) Yashima, E.; Maeda, K.; Sato, O. *J. Am. Chem. Soc.* **2001**, *123*, 8159−8160. (c) Yashima, E.; Maeda, K.; Yamanaka, T. *J. Am. Chem. Soc.* **2000**, *122*, 7813−7814. (d) Iftime, G.; Labarthet, F. L.; Natansohn, A.; Rochon, P. *J. Am. Chem. Soc.* **2000**, *122*, 12646−12650. (e) Maeda, K.; Yamamoto, N.; Okamoto, Y. *Macromolecules* **1998**, *31*, 5924−5926. (f) Yashima, E.; Maeda, K.; Okamoto, Y. *Nature* **1999**, *399*, 449−451. (g) Schlitzer, D. S.; Novak, B. M. *J. Am. Chem. Soc.* **1998**, *120*, 2196−2197.
(16) Shinkai, S.; Manabe, O. *Top. Curr. Chem.* **1984**, *121*, 67−104.
(17) Ueno, A.; Tomita, Y.; Osa, T. *Tetrahedron Lett.* **1983**, *24*, 5245−5248.
(18) (a) Agai, S.; Karatsu, T.; Kitamura, A. *Chem. Eur. J.* **2005**, *11*, 4054−4063. (b) Yagai, S.; Nakajima, T.; Karatsu, T.; Saitow, K.; Kitamura, A. *J. Am. Chem. Soc.* **2004**, *126*, 11500−11508. (c) Kawasaki, T.; Tokuhiro, M.; Kimizuka, N.; Kunitake, T. *J. Am. Chem. Soc.* **2001**, *123*, 6792−6800.

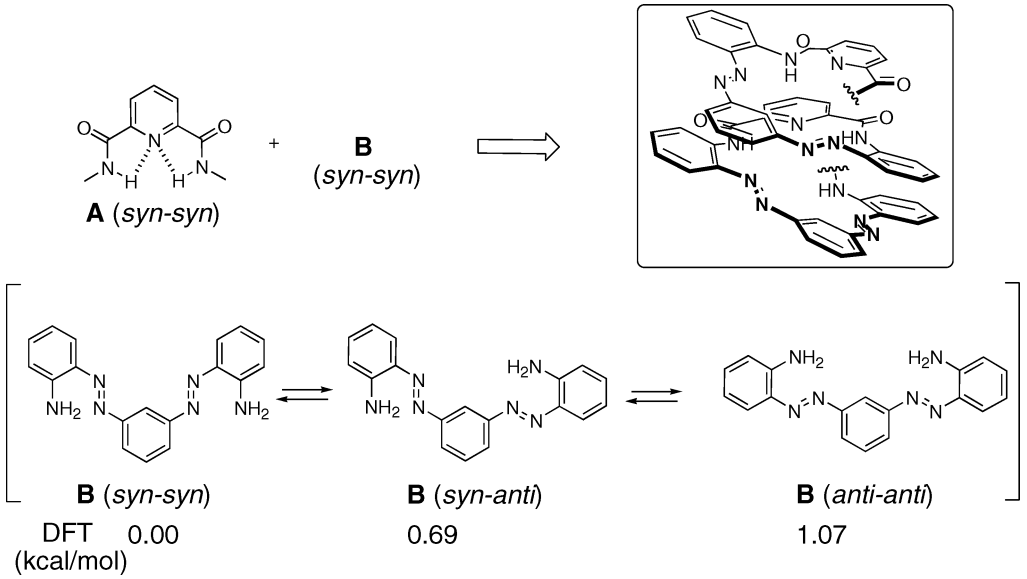

Figure 1. Design of helical azobenzene oligomer.

as a structural component of the backbone wherein the *trans* azo bond is geometrically required for helicity.

Design Considerations and Molecular Modeling

The oligomers in this work were designed based on two primary considerations: (1) the oligomers should adopt a "compact" helical conformation when the azobenzene moiety is in the more stable *E* form to facilitate conformational characterization, and (2) the *E* → Z isomerization should potentially disrupt the helicity of the oligomer. Monte Carlo conformational searching using the Amber* force field predicted that oligomers composed of alternating sequences of pyridine-2,6-dicarboxamides (**A**) and *meta*-(phenylazo)azobenzene (**B**) monomers adopt extended two- or four-turn helical conformations in oligomers **8** and **9** (shown in Scheme 1), respectively, when all azo bonds are in the more stable *E* geometry (Figures 1 and 2).

Folding into a helical conformation requires both the pyridine-2,6-dicarboxamides and the (phenylazo)azobenzenes to adopt *syn*−*syn* conformations (Figure 1). Prior density functional theory (DFT) computational studies indicated that the *syn*−*syn* conformation in pyridine-2,6-dicarboxamides is preferred over the *syn*−*anti* and *anti*−*anti* conformations by 6.3 and 10.1 kcal/mol, respectively.[4] The *syn*−*syn* conformation places the amide NH groups in close proximity to the pyridine-*N*, which permits intramolecular hydrogen bonding interactions to occur and minimizes the repulsive electrostatic interactions between the amide oxygens and the pyr-*N* that are present in the *anti*−*anti* and *syn*−*anti* forms.[20,21] However, Monte Carlo conformational searching followed by DFT geometry optimization and single point energy calculations performed at the B3LYP/6-311++G**//

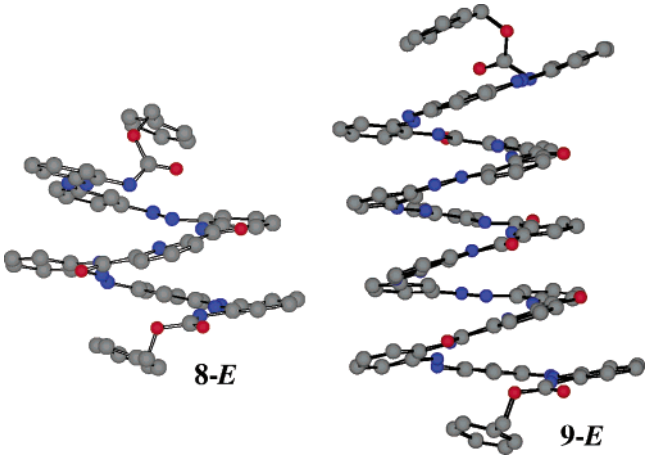

Figure 2. Lowest energy conformations of the *E* forms of oligomers **8** and **9** predicted by Monte Carlo conformational searching using the Amber* force field.

B3LYP/6-311G* levels of theory[22] revealed a relatively small preference for the *syn*−*syn* conformation of (phenylazo)-azobenzene **B**.

Nevertheless, Monte Carlo conformational searching of oligomers **8** and **9** suggests that pyridine-2,6-dicarboxamide and phenylazo(azobenzene) repeat units will adopt *syn*−*syn* conformations within the helices. Accordingly, oligomers of **A** and **B** were expected to adopt a compact helical conformation in the *E*-azo geometry, whereas photoisomerization of a portion of the azo bonds to a *Z* geometry would perturb the helical conformational preference.

Results and Discussion

Synthesis. Reaction of *m*-phenylenediamine **3** with 2 equiv of an arylnitroso species would provide the most efficient

(19) (a) Ghosh, S.; Banthia, A. K.; Chen, Z. *Tetrahedron* **2005**, *61*, 2889−2896. (b) Liao, L.-X.; Stellacci, F.; McGrath, D. V. *J. Am. Chem. Soc.* **2004**, *126*, 2181−2185. (c) Momotake, A.; Arai, T. *Polymer* **2004**, *45*, 5369−5390. (d) Wang, S.; Wang, X.; Li, L.; Advincula, R. C. *J. Org. Chem.* **2004**, *69*, 9073−9084. (e) Grebel-Koehler, D.; Liu, D.; De Feyter, S.; Enkelmann, V.; Weil, T.; Engels, C.; Samyn, C.; Muellen, K.; De Schryver, F. C. *Macromolecules* **2003**, *36*, 578−590. (f) Archut, A.; Azzellini, G. C.; Balzani, V.; Cola, L.; Voegtle, F. *J. Am. Chem. Soc.* **1998**, *120*, 12187−12191. (g) Archut, A.; Vogtle, F.; De Cola, L.; Azzellini, G. C.; Balzani, V.; Ramanujam, P. S.; Berg, R. H. *Chem. Eur. J.* **1998**, *4*, 699−706.

(20) (a) Huang, B.; Prantil, M. A.; Gustafson, T. L.; Parquette, J. R. *J. Am. Chem. Soc.* **2003**, *125*, 14518−14530. (b) Huang, B.; Parquette, J. R. *J. Am. Chem. Soc.* **2001**, *123*, 2689−2690. (c) Recker, J.; Tomcik, D. J.; Parquette, J. R. *J. Am. Chem. Soc.* **2000**, *122*, 10298−10307.

(21) (a) Hamuro, Y.; Geib, S. J.; Hamilton, A. D. *J. Am. Chem. Soc.* **1997**, *119*, 10587−10593. (b) Hamuro, Y.; Geib, S. J.; Hamilton, A. D. *J. Am. Chem. Soc.* **1996**, *118*, 7529−7541.

(22) Frisch, M. J.; et al. *Gaussian 03*, revision B.04; Gaussian, Inc.: Pittsburgh, PA, 2003.

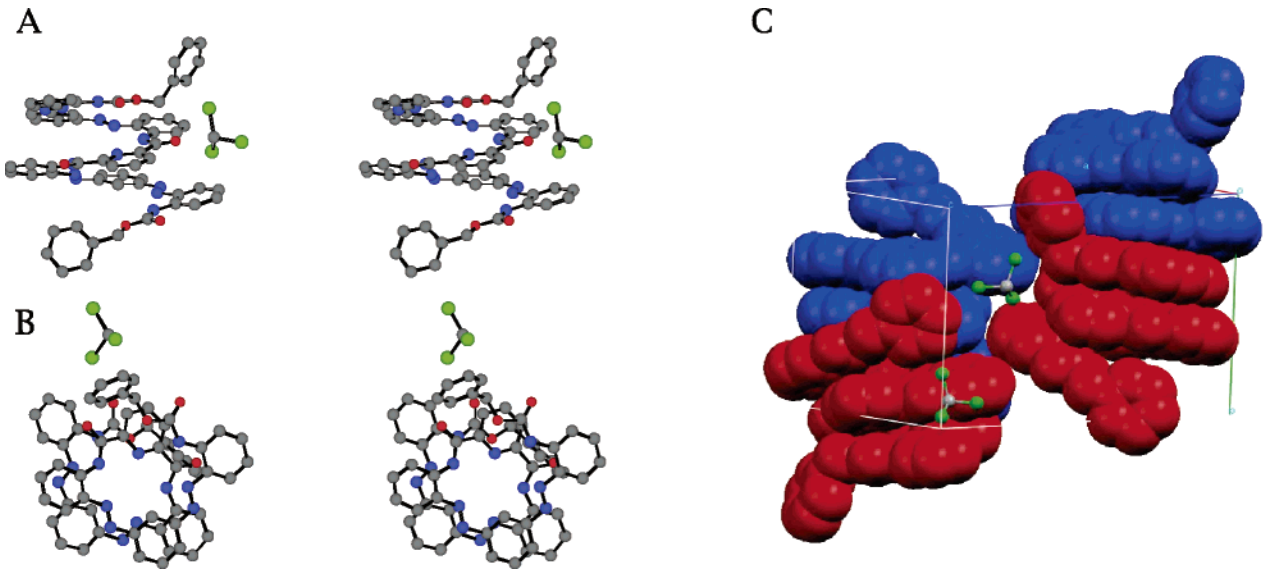

Figure 3. X-ray structure of **8** (a) side-on and (b) top-down views, (c) unit cell containing two right- and two left-handed molecules stacked in columns.

method to obtain (phenylazo)azobenzene **7** (Scheme 1). However, mixing 2 equiv of *N*-(2-nitrosophenyl)acetamide **2**, prepared by acetylation of 2-nitroaniline **1** followed by reduction of the nitro group with hydrazine over Rh−C and oxidation with *t*-C_4H_9OCl, and *m*-phenylenediamine **3** in the presence of acetic acid produced an unidentified water-soluble product mixture. Reasoning that the electron-rich nature of *m*-phenylenediamine was causing reaction to take place on the aromatic ring in addition to the amino groups, 3-nitroaniline **4a** was condensed with **2** in acetic acid at 100 °C, providing *N*-[2-(3-nitrophenylazo)phenyl]acetamide **5a** in 60% yield.[23] However, reduction of the nitro group to the corresponding amine with NaHS in ethanol/water[24] provided variable yields ranging from 10 to 60% due to competitive reduction of the azo function. Employing Na_2S[25] or $(NH_4)_2S$ similarly afforded azo bond cleavage products. Therefore, to avoid the requirement for a selective nitro reduction, 3-allyloxycarbamate (**4b**) and 3-phthalimide (**4c**) derivatives of *m*-phenylenediamine were investigated as electron-deficient analogues of 3-nitroaniline that could be chemoselectively deprotected without competitive azo bond reduction. Whereas the 3-allyloxycarbamate **4b** provided only 20% yield of **5b** in the coupling event, the more electron-deficient 3-phthalimide system (**4c**) provided a high yield of azobenzene **5c**. Selective deprotection of the phthalimide group was achieved using aqueous methylamine, affording 68% yield of **6** over the two steps. Subsequent condensation of amine **6** with nitroso **2** in acetic acid afforded (phenylazo)azobenzene **7a** in 54% yield. Hydrolysis of the acetamide groups with KOH in ethanol/water followed by monoprotection with benzylchloroformate provided monoamine **7c**. Amidation of pyridine-2,6-dicarbonyl dichloride with 2 equiv of **7c** afforded first generation oligomer **8** in 50% yield. Removal of the benzyloxycarbonyl (CBz) groups was achieved without concomitant azo reduction using thioanisole in trifluoroacetic acid[26] in 95% yield. Growth to the second generation oligomer **9** occurred by repetition of the monoprotection/amidation sequence.

Table 1. Chemical Shifts of Protons **Ha**−**Hf** in **7**−**9** in Various Solvents at 25 °C

solvent	compound	Ha	Hb	Hc	Hd	He	Hf
$CDCl_3$	**7d**	9.48	8.35				
	7e	12.50	8.92				
	8	9.37	7.99	11.76			
	9	9.15	7.62	11.08	10.83	7.39	10.59
C_6D_6	**7d**	9.65	8.36				
	7e	12.69	9.18				
	8	9.52	8.10	11.73			
	9	9.40	7.88	11.28	11.07	7.88	10.96
CCl_4[a]	**7d**	9.49	8.19				
	7e	12.16	8.77				
	8	9.15	7.82	11.50			
	9	9.02	7.51	10.90	10.59	7.26	10.44
DMSO-d_6	**7d**	9.83	8.51				
	7e	12.35	8.77				
	8	9.48	7.98	11.65			
	9	9.21	7.56	11.00	10.67	7.25	10.50

[a] 2% C_6D_6 used for signal locking.

X-ray Structure: Solid State Conformation of 8. A clear, orange plate-like crystal (monoclinic, space group $P2_1/n$) of oligomer **8** was obtained by slow evaporation of a $CHCl_3$ solution.[27] The crystal structure indicated that the oligomer adopts a two-turn helical conformation with a helical pitch of approximately 3.4 Å in the solid state (Figure 3A,B). It is noteworthy that, with the exception of the orientation of the terminal benzyloxycarbonyl groups, the crystal structure virtually superimposes with the calculated structure of **8** shown in Figure 2. The pyridyl-2,6-dicarboxamide and phenylazo(azobenzene) building blocks adopt the expected *syn*−*syn* forms in the solid-state helical structure, wherein both pyridyl amide NHs point inwardly toward the helix interior, forming intramolecular hydrogen bonds with both the pyridine-*N* and an adjacent azo

(23) Nutting, W. H.; Jewell, R. A.; Rapoport, H. *J. Org. Chem.* **1970**, *35*, 505−508.
(24) (a) Ueno, K. *J. Am. Chem. Soc.* **1952**, *74*, 4508−4511. (b) Ruggli, P.; Wust, W. *Helv. Chim. Acta* **1945**, *28*, 781−791. (c) Asanuma, H.; Liang, X.; Komiyama, M. *Tetrahedron Lett.* **2000**, *41*, 1055−1058. (d) Manka, J. T.; Guo, F.; Huang, J.; Yin, H.; Farrar, J. M.; Sienkowska, M.; Benin, V.; Kaszynski, P. *J. Org. Chem.* **2003**, *68*, 9574−9588. (e) Asanuma, H.; Liang, X.; Komiyama, M. *Tetrahedron Lett.* **2000**, *41*, 1055−1058.
(25) Singh, J.; Singh, P.; Boivin, J. L.; Gagnon, P. E. *Can. J. Chem.* **1962**, *40*, 1921−1925.
(26) Kiso, Y.; Ukawa, K.; Akita, T. *Chem. Commun.* **1980**, 101−102.
(27) Crystallographic details: $C_{59}H_{45}N_{13}O_6$ with $CHCl_3$, FW = 1151.45, monoclinic, $P2_1/n$, a = 16.117(2) Å, b = 13.657(2) Å, c = 25.154(3), β = 98.734(6)°, T = 150(2) K, Z = 4, Mo Kα radiation, $R1$ (on 9650 reflections, all data) = 0.089, $wR2$ (all data) = 0.145, $R1$ (on 6494 reflections with $I > 2\sigma(I)$) = 0.053, GOF on F^2 = 1.042.

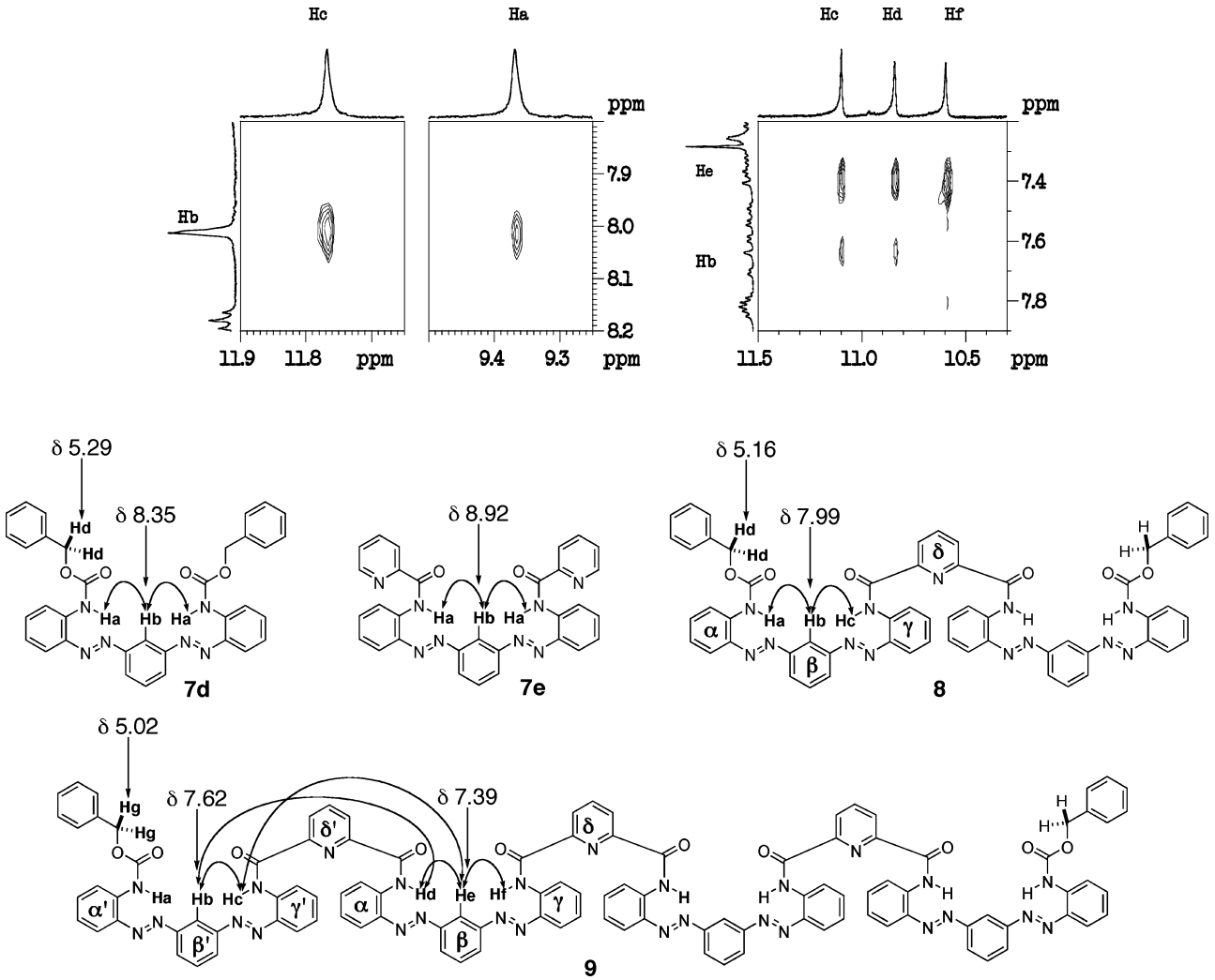

Figure 4. Two-dimensional ^{1}H−^{1}H NOESY spectra of **8** (top left) and **9** (top right) in $CDCl_3$, and anisotropic shifting of **Hb** in **8** and **9** compared with model compounds for terminal (**7d**) and internal (**7e**) positions.

nitrogen. The helical conformation induces offset face-to-face π-stacking interactions between the 1,3-diazobenzene and 2-acylaminophenylazo rings on adjacent turns of the helix with closest edge distances of 3.53 Å. The unit cell contains four molecules of **8**, each with an associated $CHCl_3$ molecule, that exist in two right- and two left-handed helical forms. The molecules assemble into stacked columns of helices in the crystal lattice in which each column contains a single helical sense (Figure 3).[28]

^{1}H NMR Spectroscopy. The ^{1}H NMR spectra of **8** and **9** displayed several attributes consistent with the presence of an extended helical conformation in polar and nonpolar solvents. Significant upfield shifts of several proton resonances were observed in $CDCl_3$, C_6D_6, CCl_4, and DMSO-d_6 due to the anisotropic shielding of the stacked aromatic rings in the helical structure (Table 1).[21,28] For example, in $CDCl_3$, the proton resonance ortho to both azo bonds (**Hb**) in the terminal β-rings shifted progressively upfield as oligomer length was increased: **7d** (δ_{Hb} 8.35)/**7e** (δ_{Hb} 8.92) → **8** (δ_{Hb} 7.99) → **9** (δ_{Hb} 7.62) (Figure 4). Similarly, the β-ring proton resonance located nearer the center of oligomer **9** (**He**) occurred 0.23 ppm upfield of the related β-ring proton at the terminal position (**Hb**), and 1.53 ppm upfield of **Hb** in model **7e**. Similar upfield shifts were observed even in DMSO-d_6. Therefore, despite the chemical similarity of many of the protons within the oligomer, the increased upfield shifting observed nearer the center of the oligomer chain resulted in spectra displaying highly dispersed resonances for most of the protons. Accordingly, all the proton resonances of **8** and **9** could be assigned using 2-D COSY and selective TOCSY NMR experiments (Supporting Information). Furthermore, NOE enhancements were observed between protons oriented toward the center of the helix in $CDCl_3$ (Figure 4). For example, the NOESY spectrum of oligomer **8** displayed cross-peaks between **Hb** and the amide protons **Ha** and **Hc**, positioned above and below the plane of **Hb** in the helix. These cross-peaks were also observed in the NOESY spectrum of **7d** and **7e**. Although the proximity of **Ha**−**Hc** is consistent with the presence of a helical structure in **8**, these cross-peaks do not rule out a nonhelical conformation of **8** wherein **Ha**−**Hc** are positioned as in **7d/e**. In contrast, the NOESY spectrum of **9** revealed cross-peaks supporting a helical conformational preference in $CDCl_3$. For example, proton **He**, located on the interior β-ring, exhibited cross-peaks with the amide protons located in regions above (**Hd** and **Hc**) and below (**Hf**) its

(28) Ohkita, M.; Lehn, J.-M.; Baum, G.; Fenske, D. *Chem. Eur. J.* **1999**, *5*, 3471−3481.

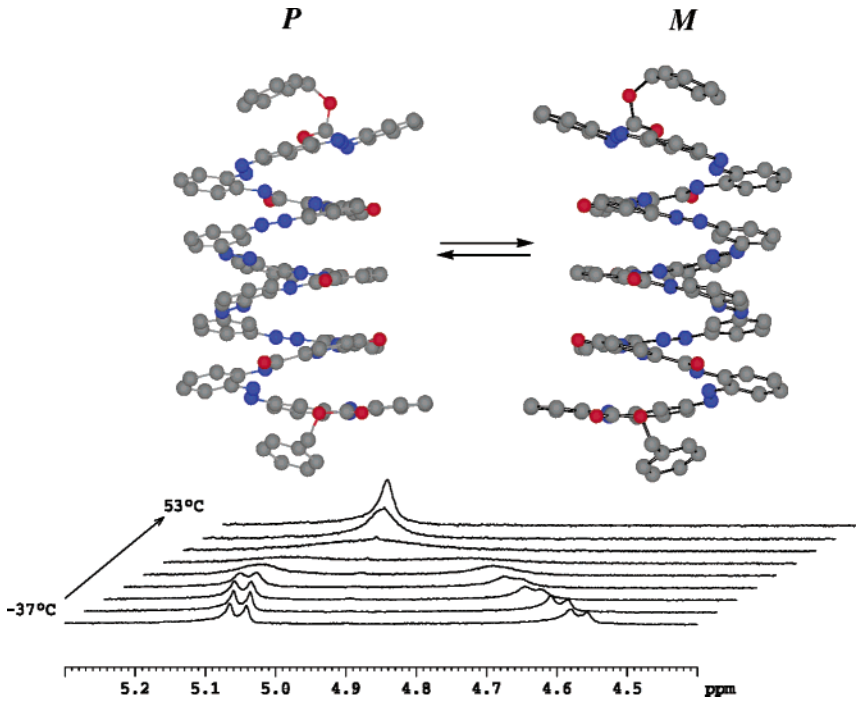

Figure 5. Determination of helical interconversion barrier of **9** in $CDCl_3$ using ^1H NMR line shape analysis of resonances for CBz methylene (**Hg**) protons.

position in the helix in **9**. Similarly, the terminal β'-ring proton **Hb** exhibited cross-peaks with amide protons **Hc** and **Hd**. Identical cross-peaks were also observed for oligomer **9** in DMSO-d_6, indicating that the helical conformation is similarly adopted in polar, aprotic media (Supporting Information).

Helical Interconversion Barrier. In the absence of a chiral, nonracemic perturbation, the helical conformations exist as an interconverting mixture of equal amounts of *M* and *P* helices. Accordingly, the dynamic helical interconversion of oligomers **8** and **9** was observable in the ^1H NMR spectra in several solvents.[29] For example, at lower temperatures in $CDCl_3$, the methylene hydrogens (**Hd** in **8**; **Hg** in **9**) of the benzyloxycarbonyl chain ends appeared as two well-separated AB-type doublets (**8**, $\Delta\nu = 106.6$ Hz; **9**, $\Delta\nu = 134.2$ Hz) due to the global helical conformation of the molecule (Figure 5). Increasing temperature caused the two doublets to gradually coalesce into a singlet, consistent with the progressive averaging of the two protons undergoing A−B exchange due to an $M \leftrightarrow P$ helical interconversion. The coalescence temperature was significantly lower for the shorter oligomer **8** (ca. −37 °C) than for **9** (ca. 23 °C) in $CDCl_3$. Similar dynamic behavior was observed in the ^1H NMR spectra of **9** in polar and nonpolar solvents (Table 2).[30] However, both the A and B proton chemical shifts as well as the difference between them ($\delta_A - \delta_B$) varied with temperature. Therefore, to calculate the rate constants for interconversion, it was necessary to estimate the intrinsic $\delta_A - \delta_B$ at a temperature where signal averaging was observed.[31] This was done by plotting the observed $\delta_A - \delta_B$ values over the temperature range in which an AB spectrum could be discerned and then extrapolating to a temperature at which A−B averaging takes place. A−B line shapes were then calculated as a function of k_1, the rate constant for helical interconversion using the observed J_{A-B} coupling constant (**8**, 11.6 Hz; **9**, 11.7 Hz). Matching the experimental and calculated NMR spectra provided the first-order rate constant for helical interconversion at various temperatures. Thus $\Delta H^{\ddagger}$ and $\Delta S^{\ddagger}$ were obtained from a plot according to the following equation: $\ln(k/T) = -\Delta H^{\ddagger}/RT + \Delta S^{\ddagger}/R + 23.76$. Accordingly, helical exchange barriers ($\Delta G^{\ddagger}$) were 11.1 and 13.8 kcal/mol for **8** and **9**, respectively, in $CDCl_3$. The *M*−*P* barrier of oligomer **9** was slightly higher in DMSO-d_6 but did not vary significantly among nonpolar solvents (Table 2). The similar helical interconversion barriers for **8** and **9** suggests a stepwise unfolding mechanism for helical interconversion rather than a global wrap−unwrap process.[28]

Table 2. Kinetic Parameters of Helical Interconversion

oligo	solvent	$\Delta H^{\ddagger}$ (kcal/mol)	$\Delta S^{\ddagger}$ (cal·mol^{-1}·K^{-1})	T_c (K)	$\Delta G^{\ddagger}(T_c)$ (kcal/mol)	$k(T_c)$ (s^{-1})
8[a]	$CDCl_3$	6.5 ± 0.4	−19.4 ± 1.6	236	11.1	276
9	$CDCl_3$	11.8 ± 1.8	−6.6 ± 6.2	296	13.8	435
9	C_6D_6	20.2 ± 2.4	22.0 ± 8.2	295	13.7	443
9	CCl_4[b]	22.3 ± 1.8	28.6 ± 6.3	305	13.6	1178
9	DMSO-d_6	28.2 ± 1.8	44.6 ± 5.9	313	14.3	729

[a] See ref 30. [b] 2% C_6D_6 used for signal locking.

Photoisomerization Studies. Azobenzene containing building blocks **6**−**7**(**a**−**e**) and oligomers **8**−**9** exhibited similar UV−vis absorption spectra (Figure 6 and Supporting Information). Whereas unsubstituted *E*-azobenzene displays a strong $\pi \rightarrow \pi^*$ absorption at 320 nm and a weak $n \rightarrow \pi^*$ transition at 440 nm,[32] the *o*-acylamino substitution present in structures **6**−**9** induced a large red-shift of the $\pi \rightarrow \pi^*$ band to 390 nm, causing the long wavelength component of this transition to overlap with the $n \rightarrow \pi^*$ band centered at ca. 450 nm.[33] Accordingly, irradiation of oligomers **8** and **9** with 350 or 410 nm light

(29) Preston, A. J.; Fraenkel, G.; Chow, A.; Gallucci, J. C.; Parquette, J. R. *J. Org. Chem.* **2003**, *68*, 22−26.
(30) The lower coalescence temperature of **8** precluded determination of the helical interconversion barrier in CCl_4, C_6D_6, and DMSO-d_6, which freeze in that temperature range.
(31) Kaplan, J. I.; Fraenkel, G. *NMR of Chemically Exchanging Systems*; Academic Press: New York, 1960; pp 101−104.
(32) Griffiths, J. *Chem. Soc. Rev.* **1972**, *1*, 481−493.
(33) Hirose, Y.; Yui, H.; Sawada, T. *J. Phys. Chem. A* **2002**, *106*, 3067−3071.

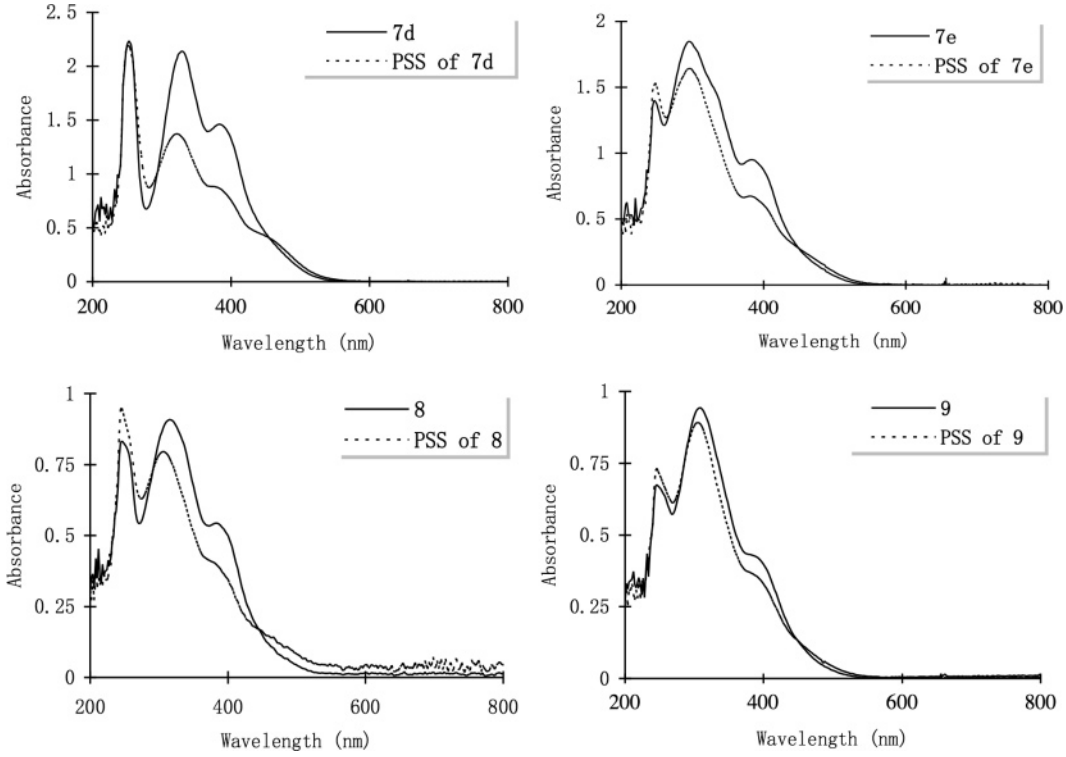

Figure 6. UV−vis spectra of **7d**,**e** and **8**−**9** before and at the photostationary state (PSS) after irradiation with 350 nm light for 10 min.

Table 3. Percent *Z*-Isomer at PSS by UV and ^{1}H NMR[a]

compound	% *Z* (UV)[b]	% *Z* (NMR)[c]	% *Z* (int.) (NMR)[c]	% Z (term.) (NMR)[c]
6	65	71		
7a	56	63		
7d	41	53		
7e	30	39		
8	29	33	25	41
9	17	∼20	<15	39

[a] Ratios measured within 10 min following irradiation. [b] PSS attained within 10 min for UV. [c] PSS attained within 1 h for ^{1}H NMR experiments.

induced an $E \rightarrow Z$ isomerization to take place, as evidenced by a decrease in the 390 nm absorption, an increase in absorbance at 450 nm, and a color change from yellow to orange. A photostationary state (PSS) was reached for **7**−**9** within 10 min of irradiation at micromolar concentrations by UV−vis spectroscopy and within 1 h at the millimolar concentrations employed for NMR analysis. The content of *Z*-isomer at PSS was determined using ^{1}H NMR and by UV−vis spectra using the formula $(A_0 - A_{PSS(390)}/A_0)$, where A_0 and $A_{PSS(390)}$ represent the absorbances at 390 nm before and after irradiation with UV light, respectively. This formula assumes a negligible absorption of the *Z*-isomer at 390 nm. The slightly lower *Z*-isomer content determined by UV−vis spectroscopy, compared with ^{1}H NMR analysis, suggests a minor absorption of the *Z*-isomer at 390 nm (Table 3). Irradiation of **8**/**9** with either 350 or 410 nm light afforded similar *Z*/*E* ratios at the PSS after ca. 10 min. However, in contrast to irradiation with 350 nm light, exposure of **8** or **9** to 410 nm light for longer than 10 min caused an irreversible disappearance of starting material that was competitive with $E \rightarrow Z$ isomerization and was accompanied by the development of a colorless, transparent solution. The photobleaching that occurred at 410 nm was most likely due to a competitive photoreduction of the azo function and did not occur upon exposure to 350 nm light.[34] Accordingly, whereas irradiation of monoazobenzene **6** at 350 nm afforded a PSS after 10 min containing 71% *Z*-isomer, photoisomerization of **8** and **9** at 350 nm provided a PSS containing only 33 and ca. 20% of the *Z*-isomer, respectively.

Effect of Structure on Photoresponsive Properties. Ortho-amino azobenzenes typically exhibit extremely fast thermal $Z \rightarrow E$ isomerization rates because delocalization of the amine lone pairs reduces the bond order of the azo bond, thereby effectively rendering the absorption spectra unresponsive to irradiation.[35] Therefore, bis(2-aminophenylazo)azobenzene **7b** did not undergo any apparent isomerization upon irradiation with 350 nm light, as determined by ^{1}H NMR and UV−vis spectroscopy. However, the corresponding bisacetyl (**7a**), bis-benzyloxycarbonyl (**7d**), and bis(2-pyridylcarboxamide) (**7e**) derivatives afforded 63, 53, and 39% *Z*-isomer at the PSS, respectively (Table 3). Whereas the *Z*-isomer content at the PSS of **7a**,**b** and **7d** generally increases as the electron-withdrawing ability of the group on nitrogen increases going from **7b** → **7d** → **7a**, the lower *Z*-isomer content of **7e** is likely a consequence of the intramolecular hydrogen bond between the amide N−H and the pyridine-*N*, which polarizes the N−H bond. Overall, $E \rightarrow Z$ photoisomerism was progressively suppressed as oligomer length increased going from **7** → **8** → **9**.[36] The $Z \rightarrow E$ isomerization rates of **7**−**9** were in the range of 10^{-5} s^{-1} at room temperature, indicating that the suppressed isomerization

(34) (a) Irick, G., Jr.; Pacifici, J. G. *Tetrahedron Lett.* **1969**, 1303−1306. (b) Pacifici, J. G.; Irick, G., Jr. *Tetrahedron Lett.* **1969**, 2207−2210. (c) Albini, A.; Fasani, E.; Pietra, S. *Perkin Trans. 2* **1982**, 1393−1395. (d) Albini, A.; Fasani, E.; Pietra, S. *Perkin Trans. 2* **1983**, 1021−1024.
(35) Sawicki, E. *J. Org. Chem.* **1957**, *22*, 1084−1088.
(36) For examples of suppressed photoisomerization, see: (a) (hydrogen-bonded rosette) Yagai, S.; Nakajima, T.; Karatsu, T.; Saitow, K.; Kitamura, A. *J. Am. Chem. Soc.* **2004**, *126*, 11500−11508. (b) (dendrimer) Momotake, A.; Arai, T. *Tetrahedron Lett.* **2004**, *45*, 4131−4134.

was not due to fast thermal reversion to the *E* form (Supporting Information).

Closer inspection of the ^{1}H NMR spectra of structures **6**−**8** before and after irradiation provided information about how the position within the helix structure affected the *Z*/*E* ratio of a particular azo function. As shown in Figure 7, irradiation of azobenzene **6**, having a single azo bond, produced a spectrum displaying the amide N−H peak for the *Z*-isomer that was shifted upfield by 1.9 ppm relative to the *E* form, corresponding to 71% *Z*, in accord with the ratio determined by UV−vis. Acetyl-protected **7a**, having two azo bonds, produced three isomers (*E*/*E*, *Z*/*E*, *Z*/*Z*) following irradiation, exhibiting a similar upfield shifting of the N−H peaks adjacent to *Z*-azo bonds. Accordingly, the *E*/*E* and *Z*/*Z* forms featured a single N−H resonance at δ 10.13 and 8.21, respectively, whereas the *Z*/*E* isomer exhibited separate N−H peaks at δ 9.95 and 8.30. The upfield shifting of N−H resonances adjacent to *Z*-azo bonds also occurred in the spectra of in Cbz-protected **7d** and 2-pyridylcarboxamide derivative **7e**. However, N−Hs adjacent to the pyridyl-*N* in **7e** were shifted downfield by ca. 3 ppm relative to the corresponding CBz N−Hs present in **7d**. Accordingly, the downfield shifting of pyridylcarboxamide N−Hs in conjunction with the upfield shifting of N−Hs adjacent to *Z*-azo bonds facilitated the independent determination of the *Z*/*E* ratios of the terminal and internal azo bonds in the more complicated spectra of oligomers **8** and **9**. Integration of these peaks indicated that whereas the terminal azo bonds adjacent to the CBz groups in both **8** and **9** experienced ca. 40% isomerization to the *Z* form, similar to **7d**, the internal azo bonds were converted to 25% *Z* in **8** and <15% *Z* in **9**, corresponding to overall *Z*/*E* ratios of 33/67 and 20/80 for **8** and **9**, respectively, in accord with the ratios determined by UV−vis. Therefore, the contrasting behavior of the terminal azo bonds, which afford *Z*/*E* ratios similar to those of model compound **7d**, and the internal azo groups, which exhibit significantly lower *Z*/*E* conversion ratios compared with **7e**, indicates that the electronic nature of the carboxamide group adjacent to the azo bond is not solely responsible for the suppressed $E \rightarrow Z$ isomerization in the oligomers.

The effect of $E \rightarrow Z$ isomerization on the conformation of **8** and **9** is apparent in the ^{1}H NMR spectra (Figure 8). In the more stable *E*-azobenzene geometry, both **8** and **9** exhibit well-resolved, sharp peaks for all protons except for the highly broadened resonance at δ 5.0−5.2 ppm for **9** associated with the terminal benzyloxycarbonyl methylene hydrogens due to dynamic interconversion of the *M* and *P* helical forms. Upon irradiation at 350 nm, the broad resonance at δ 5.0−5.2 ppm in oligomer **9** shifts downfield and becomes a series of sharp singlets consistent with either (1) a conversion to a nonhelical form lacking a dynamic helical equilibrium or (2) a decrease in the helical interconversion barrier. The observation that the terminal azo bonds experience increased conversions to the *Z* form supports a lowering of the helical barrier. Predominant isomerization of the terminal azo groups would lead to an effective decrease in the helix length and would afford a lower barrier to helical interconversion similar to the decreased barrier of oligomer **8** compared with that of **9**. A lowering of helix interconversion barrier is further supported by the temperature-dependent ^{1}H NMR spectra of **9** at the PSS (**9-PSS**), wherein the downfield shifted singlet at δ 5.31 for **9** becomes two AB-type doublets (J = 11.8 Hz) consistent with the presence an *M*−*P* helical interconversion in **9-PSS** (Figure 8, inset). Line shape analysis provides a helical interconversion barrier for **9-PSS** of 12.8 kcal/mol ($\Delta H^{\ddagger}$ = 6.3 ± 2.2 kcal/mol, $\Delta S^{\ddagger}$ =

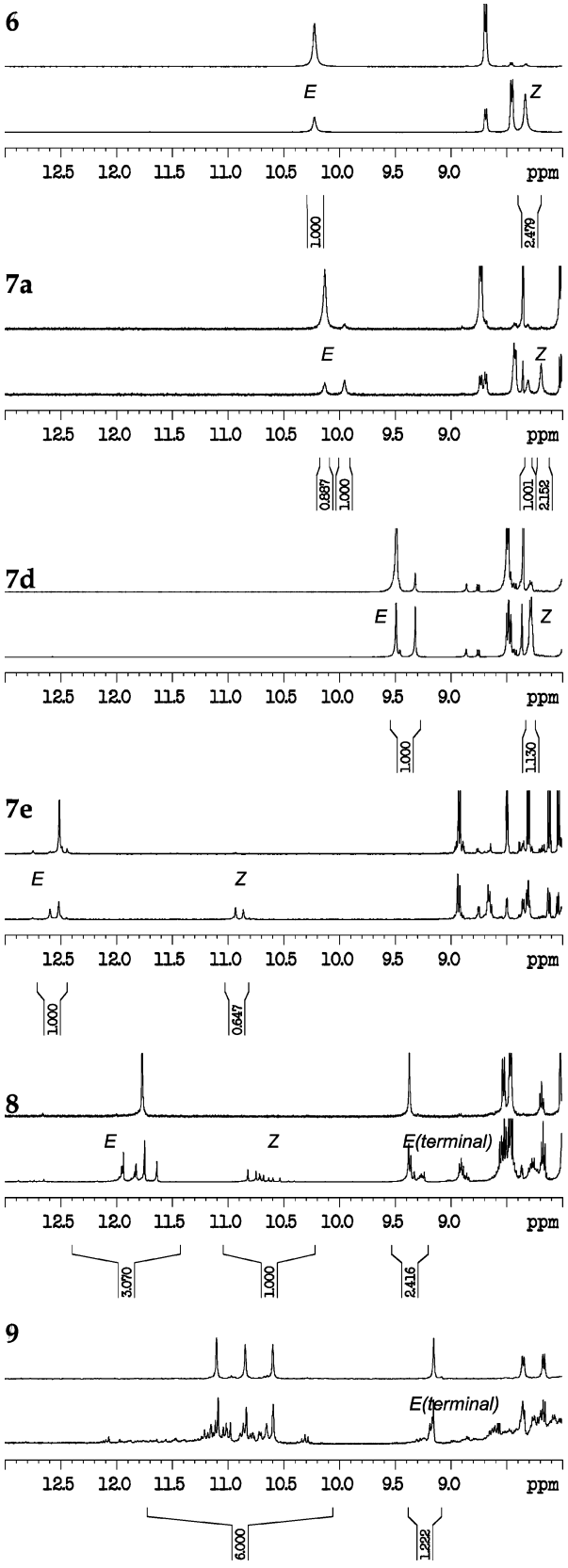

Figure 7. ^{1}H NMR spectroscopy before (top) and after irradiation (bottom) at 350 nm of **6**−**9**.

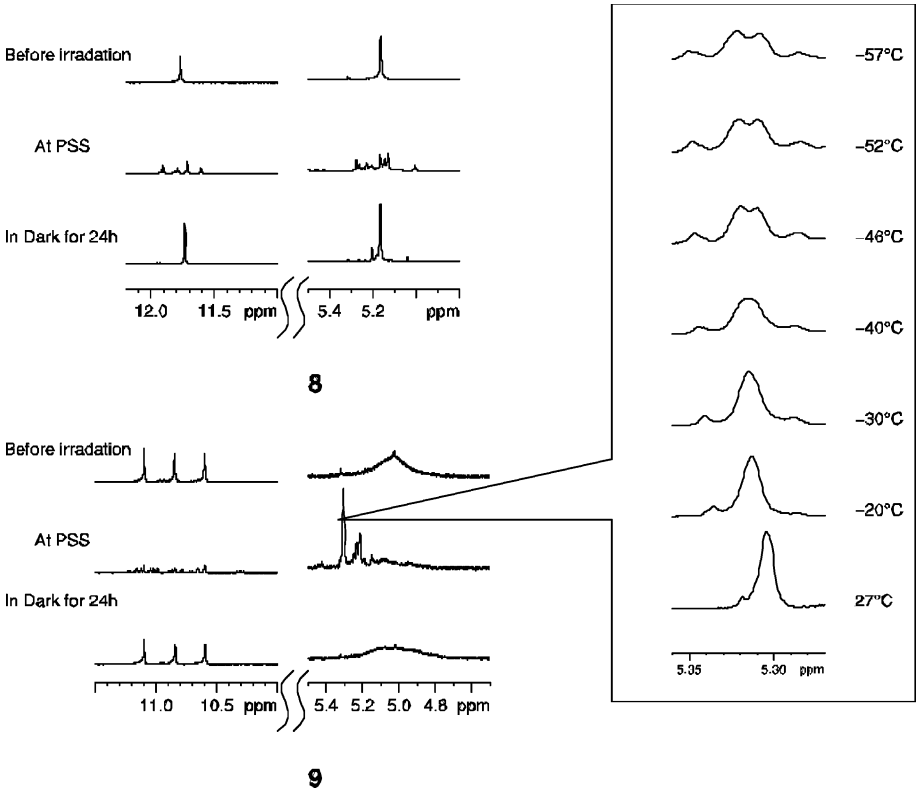

Figure 8. ^{1}H NMR spectra of **8** (top) and **9** (bottom) in $CDCl_3$ before and after irradiation (350 nm). Inset: temperature-dependent ^{1}H NMR spectra of methylene protons exhibiting A−B exchange.

Table 4. Activation Parameters in $Z \rightarrow E$ Isomerization (in CCl_4)

compound	$\Delta H^{\ddagger}$(kcal/mol)	$\Delta S^{\ddagger}$(cal·mol^{-1}·K^{-1})	$\Delta G^{\ddagger}$ (313 K) (kcal/mol)
7d[a]	22.4 ± 1.0	−4.4 ± 3.1	23.8
7e[a]	24.0 ± 1.2	0.6 ± 3.7	23.8
8[a]	16.3 ± 1.0	−24.0 ± 3.3	23.8
8[b] (terminal)	20.7 ± 2.6	−6.9 ± 8.5	22.9
8[b] (interior)	25.8 ± 2.7	9.0 ± 8.8	23.0
9[a]	18.6 ± 0.3	−16.6 ± 1.1	23.8
azobenzene (**AB**)[c]	21.9	−11.0	25.3

[a] Determined by UV−vis. [b] Determined by ^{1}H NMR. [c] From ref 40.

−25.7±9.3 cal mol^{-1} K^{-1}), which lies between the barriers determined for oligomers **8** (11.1 kcal/mol) and **9** (13.8 kcal/mol) as expected for a shorter effective helix length. Furthermore, the downfield shifting of the methylene resonance and the more similar chemical shifts of the two doublets observed for **9-PSS** ($\Delta\nu$ = 11.9 Hz), as compared with **9** ($\Delta\nu$ = 134.2 Hz), are also indicative of the predominant isomerization of the terminal azobenzene groups. This localized isomerization unwinds the ends of the helix in a manner that reduces the field anisotropy experienced by the terminal methylene protons causing the two diastereotopic methylene protons to become magnetically similar and shifted downfield.

Activation Parameters of Thermal $Z \rightarrow E$ Isomerization. The activation parameters of the thermal $Z \rightarrow E$ isomerization process were determined by measuring the apparent first-order rate constants at multiple temperatures in CCl_4[37] and plotting the Eyring equation (Table 4).[38] Thermal $Z \rightarrow E$ isomerization proceeded over several hours at room temperature with first-order rate constants in the range of 10^{-5} s^{-1} (see Supporting Information). In contrast to the structure dependence of the *Z*/*E* ratio at the PSS, the first-order rate constants and activation energies were invariant with helix length, which indicated that the isomerization of each azo linkage occurred independently. The activation energies of the terminal and internal azo bonds in oligomer **8**, determined independently by ^{1}H NMR, were similar, indicating that the suppressed photoisomerization of the internal azo functions was not due to the occurrence of a particularly fast thermal back isomerization. A plot of $\Delta H^{\ddagger}$ versus $\Delta S^{\ddagger}$ for oligomers **7d**,**e** and **8**−**9** also revealed a strong

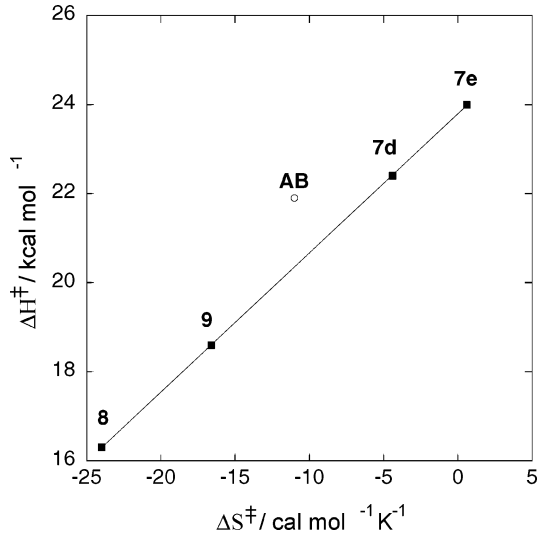

Figure 9. Plot of $\Delta H^{\ddagger}$ versus $\Delta S^{\ddagger}$.

(37) CCl_4 was chosen to minimize acid catalysis of the $Z \rightarrow E$ isomerization. See refs 35 and 40.

(38) Eyring, H. *Chem. Rev.* **1935**, *35*, 65−77.

compensation relationship with good linearity ($r = 0.999$) (Figure 9). This linear relationship suggests that the $Z \rightarrow E$ isomerization process proceeds via a single mechanism along the series.[39]

Conclusion

The synthesis, conformational properties, and photoresponsive behavior of a series of oligomers constructed using azobenzenes as a structural component geometrically required for folding have been described. The oligomers adopt multi-turn helical conformations in the solid state that are stable in both polar and nonpolar solvents when in the *E* form. The helices undergo a dynamic $M-P$ helical interconversion with energetic barriers that increase with helix length. However, the moderate increase in barrier with length is consistent with a stepwise unwinding pathway for helical exchange. Irradiation with 350 nm light provides a photostationary state in which azo bonds at the helix termini undergo greater $E \rightarrow Z$ conversions than the internal azo bonds. Accordingly, photoisomerization reduces the effective helix length, thereby lowering the $M-P$ interconversion barrier. The dynamic helical conformational equilibria offer the potential to bias the helicity via local chiral, nonracemic perturbations in future studies. Furthermore, the photoresponsive nature of the helical barrier suggests a potential to modulate chiral amplification and memory effects in longer oligomers, with higher interconversion barriers, using light.

Acknowledgment. This work was supported by the National Science Foundation (CHE-0239871). Acknowledgment is made to the donors of the American Chemical Society Petroleum Research Fund for partial support of this research.

Supporting Information Available: Experimental procedures and compound characterization for all compounds, 1D selective TOCSY NMR spectra of **7d**, **7e**, **8**, and **9**; 2D COESY spectra of **8** and **9**; NOESY spectrum of **9** in DMSO-d_6; thermal $Z \rightarrow E$ isomerization rates at various temperatures; UV−vis spectra of compounds **6**−**9** before and after photoirradiation; crystallographic information for **8**; and complete ref 22. This material is available free of charge via the Internet at http://pubs.acs.org.

JA0547228

(39) For other examples of the mechanistic significance of enthalpy−entropy compensation in azobenzene isomerism, see: (a) Norikane, Y.; Kitamoto, K.; Tamaoki, N. *J. Org. Chem.* **2003**, *68*, 8291−8304. (b) Wei, W.-h.; Tomohiro, T.; Kodaka, M.; Okuno, H. *J. Org. Chem.* **2000**, *65*, 8979−8987. (c) Asano, T.; Okada, T.; Shinkai, S.; Shigematsu, K.; Kusano, Y.; Manabe, O. *J. Am. Chem. Soc.* **1981**, *103*, 5161−5165. (d) Nishimura, N.; Sueyoshi, T.; Yamanaka, H.; Imai, E.; Yamamoto, S.; Hasegawa, S. *Bull. Chem. Soc. Jpn.* **1976**, *49*, 1381−1387.

(40) Brown, E. V.; Granneman, G. R. *J. Am. Chem. Soc.* **1975**, *97*, 621−627.